Journal of Pharmaceutical Analysis 13 (2023) 1548–1561

Contents lists available at ScienceDirect

Journal of Pharmaceutical Analysis

journal homepage: www.elsevier.com/locate/jpa

Original article

Glutaredoxin-1 alleviates acetaminophen-induced liver injury by decreasing its toxic metabolites

Ying Xu [1], Yan Xia [1], Qinhui Liu, Xiandan Jing, Qin Tang, Jinhang Zhang, Qingyi Jia, Zijing Zhang, Jiahui Li, Jiahao Chen, Yimin Xiong, Yanping Li**, Jinhan He*

Department of Pharmacy, Institute of Metabolic Diseases and Pharmacotherapy, West China Hospital, Sichuan University, Chengdu, 610041, China

ARTICLE INFO

Article history:
Received 21 April 2023
Received in revised form
6 July 2023
Accepted 7 August 2023
Available online 9 August 2023

Keywords:
Glutaredoxin-1
S-glutathionylation
Acetaminophen
Toxic metabolites
Cyp3a11

ABSTRACT

Excessive *N*-acetyl-*p*-benzoquinone imine (NAPQI) formation is a starting event that triggers oxidative stress and subsequent hepatocyte necrosis in acetaminophen (APAP) overdose caused acute liver failure (ALF). *S*-glutathionylation is a reversible redox post-translational modification and a prospective mechanism of APAP hepatotoxicity. Glutaredoxin-1 (Glrx1), a glutathione-specific thioltransferase, is a primary enzyme to catalyze deglutathionylation. The objective of this study was to explored whether and how Glrx1 is associated with the development of ALF induced by APAP. The *Glrx1* knockout mice (*Glrx1*$^{-/-}$) and liver-specific overexpression of *Glrx1* (*AAV8-Glrx1*) mice were produced and underwent APAP-induced ALF. Pirfenidone (PFD), a potential inducer of Glrx1, was administrated preceding APAP to assess its protective effects. Our results revealed that the hepatic total protein *S*-glutathionylation (PSSG) increased and the Glrx1 level reduced in mice after APAP toxicity. *Glrx1*$^{-/-}$ mice were more sensitive to APAP overdose, with higher oxidative stress and more toxic metabolites of APAP. This was attributed to Glrx1 deficiency increasing the total hepatic PSSG and the *S*-glutathionylation of cytochrome p450 3a11 (Cyp3a11), which likely increased the activity of Cyp3a11. Conversely, *AAV8-Glrx1* mice were defended against liver damage caused by APAP overdose by inhibiting the *S*-glutathionylation and activity of Cyp3a11, which reduced the toxic metabolites of APAP and oxidative stress. PFD precede administration upregulated Glrx1 expression and alleviated APAP-induced ALF by decreasing oxidative stress. We have identified the function of Glrx1 mediated PSSG in liver injury caused by APAP overdose. Increasing Glrx1 expression may be investigated for the medical treatment of APAP-caused hepatic injury.

1. Introduction

Acetaminophen (APAP) is a common over-the-counter medication with antipyretic and analgesic effects, which is considered safe when taken at the suggested dosage. However, APAP overdose can lead to serious liver damage and even acute liver failure (ALF), occurring chronically or unintentionally, largely due to an individual taking multiple APAP-containing products at once [1]. APAP toxicity is one of the most frequent cause of acute liver injury, accounting for 40%–70% of all ALF in the United Kingdom [1], and nearly 46% in the United States [2,3]. In particular, given the global spread of coronavirus disease 2019, many patients might take multiple medications containing APAP to reduce headaches and fever, heightening the chance of APAP poisoning [4,5].

When taken at the suggested medical dosage, the liver primarily metabolizes APAP by phase II conjugating enzymes through glucuronidation and sulfation to produce non-toxic byproducts that are eliminated through urination. A small part of APAP is converted via cytochrome p450 enzymes into the harmful intermediate *N*-acetyl-*p*-benzoquinone imine (NAPQI). NAPQI detoxification is achieved by combining with glutathione (GSH). When too much APAP is taken, the phase II conjugating enzymes are saturated, and the remaining APAP is metabolized to plentiful NAPQI via cytochrome p450 enzymes, mainly by cytochrome p450 2e1 (Cyp2e1), cytochrome p450 3a11 (Cyp3a11), and cytochrome p450 1a2 (Cyp1a2). Excessive NAPQI can induce the depletion of GSH, covalently binding to proteins to form protein-adducts, particularly mitochondrial protein [6], which triggers reactive oxidative stress, mitochondrial dysfunction, and subsequently, DNA fragmentation

Peer review under responsibility of Xi'an Jiaotong University.
* Corresponding author.
** Corresponding author.
E-mail addresses: liyanping_512@163.com (Y. Li), jinhanhe@scu.edu.cn (J. He).
[1] Both authors equally contributed to this work.

https://doi.org/10.1016/j.jpha.2023.08.004

and hepatocyte necrosis [7,8]. *N*-acetylcysteine (NAC) is an antioxidant and is currently the only clinically sanctioned medicine for the medical use in treating APAP poisoning. NAC alleviates APAP induced liver injury through GSH supplementation, but its narrow therapeutic window limits its application [9,10]. Therefore, it is valuable to explore the mechanism and the possible treatment option for hepatoxicity caused by APAP overdose.

In recent years, protein post-translational modifications (PTMs) have been implicated in APAP-caused hepatic damage. Specifically, protein *S*-glutathionylation (PSSG) levels are changed on APAP-caused hepatic injury, implying that PSSG may be functionally implicated in APAP-induced hepatotoxicity [11–13]. *S*-glutathionylation is an oxidative PTM with a dynamic and reversible process, acting as a redox "switch" and playing an important role in protein function, interaction, and localization [14]. Under oxidative stress, the exposed and deprotonated active cysteines can covalent with plentiful intracellular GSH to produce PSSG [15]. *S*-glutathionylated proteins are mainly catalyzed in reverse by glutathionyl-mixed-disulfide oxidoreductases, such as glutaredoxins (Glrx) [16]. Glrx1 has a molecular weight of 12 kDa and belongs to the Glrx family. It is considered to be a major deglutathionylation enzyme that has a significant influence on redox pathway and homeostasis [15,16]. Glrx1 is highly expressed in the liver and related to liver fibrosis [17], non-alcoholic fatty liver [18,19], and alcoholic induced liver injury [20,21], but it remains uncertain whether Glrx1 participates in APAP-caused liver damage.

In this study, we established Glrx1 as a potential therapy for APAP overdose. Glrx1 knockout increased the susceptibility of mice to APAP overdose through increasing the activity of Cyp3a11 and the content of toxic metabolites of APAP, with increased *S*-glutathionylation of Cyp3a11 as a potential mechanism. Simultaneously, the liver-specific overexpression of Glrx1 was sufficient to alleviate APAP hepatotoxicity, pirfenidone (PFD), the potential inducer of Glrx1, and reduced hepatocytes necrosis, likely by increasing Glrx1 expression. In addition, our research also revealed a vital function for PSSG in hepatic injury caused by APAP.

2. Materials and methods

2.1. Materials

APAP (A7085) and type II collagenase (C0130) were provided by Sigma-Aldrich (St. Louis, MO, USA). PFD (CSN13806) was acquired from CSNpharm (Chicago, IL, USA). The standards of 3-cysteinylacetaminophen trifluoroacetic acid salt (APAP-CYS, C994750), 3-[*N*-acetyl-*L*-cystein-*S*-yl] acetaminophen (APAP-NAC, P191100), and 6'-hydroxychlorzoxazone (H825120) were obtained from Toronto Research Chemicals (Toronto, Canada). Acetaminophen glutathione disodium salt (APAP-GSH, sc-207249-CW) was obtained from Santa Cruz Biotechnology (Dallas, TX, USA), and paracetamol sulfate potassium salt (APAP-Sul, UC448) was bought from Sigma-Aldrich. Phenacetin (T0778) and chlorzoxazone (T1650) were acquired from Target Molecule Corp. (Boston, MA, USA), midazolam (H10980025) from Jiangsu Enhua Pharmaceutical Co., Ltd. (Xuzhou, China), and 1'-hydroxymidazolam (10385–1) from Cayman Chemicals (Ann Arbor, MI, USA). The antibody of c-Jun N-terminal kinase (JNK) (9252) and phospho-JNK (p-JNK) (9251) were procured from Cell Signaling Technology (Danvers, MA, USA). Anti-Glrx1 (15804-1-AP), anti-Cyp2e1 (19937-1-AP), anti-Cyp3a11 (18227-1-AP), and anti-Cyp1a2 (19936-1-AP) were procured from Proteintech (Wuhan, China). Anti-extracellular signal-regulated kinases (ERK) (sc-93) was supplied by Santa Cruz Biotechnology. Anti-β-actin (AC026), anti-phospho-ERK1-T202+ERK2-T185 (AP0485), and anti-GAPDH (AC001) were purchased from ABclonal Technology Co., Ltd. (Wuhan, China). Anti-GSH (101-A) was obtained from Virogen (Watertown, MA, USA).

2.2. Animals

The mice used in the study were C57BL/6J strain. *Glrx1*$^{-/-}$ mice were generated using the clustered regularly interspaced short palindromic repeats (CRISPR)-CRISPR-associated protein (Cas)9 technology from Shanghai Model Organisms (Shanghai, China). Six-week-old wild type (*WT*) male mice were procured from Beijing HFK Bioscience Co., Ltd. (Beijing, China). Adeno-associated virus type 8 (*AAV8*) vector containing mouse *Glrx1* (*AAV8-Glrx1*) and *AAV8* vector containing only green fluorescent protein (*AAV8-GFP*) were obtained from Beijing Hesheng Biotechnology Co., Ltd. (Beijing, China). The *AAV8-GFP* and *AAV8-Glrx1* were injected into the caudal vein, and each mouse was injected with 100 μL of 1×10^{12} vg/mL of the virus to construct specific liver overexpression mice. Mice were allowed to chew diet freely and were housed at room temperature around 25 °C, light and dark periods alternate every 12 h at West China Hospital Animal Laboratory Center (Chengdu, China). All procedures about animals were approved by the Institutional Animal Care and Use Committee of Sichuan University (Approval No.: 2020431A).

Eight-to-ten-week-old mice received 200 mg/kg body weight APAP by intraperitoneal injection after fasting for 16 h as previous study performed [22]. APAP was dissolved in saline with ultrasonic-assisted dissolution at 37 °C, and the temperature of APAP solution was maintained throughout the injection. Serum was collected from each mouse's femoral vein at 3, 6, and 12 h following APAP injection to evaluated biochemical indexes, respectively. Liver tissues were collected at 3 and 12 h following APAP injection by sacrificing mice to evaluate liver injury. A visual scheme of sample collected in is shown in Fig. S1A.

Three weeks later, after *AAV8* injection, the mice were administrated with saline or APAP (200 mg/kg body weight). In order to study the effects of PFD, after fasting for 15.5 h, mice were orally administrated CMC-Na (Veh) or PFD (250 mg/kg), and 30 min later, they were given 200 mg/kg APAP administered via intraperitoneal injection. All animals were sacrificed to obtain blood and liver at different times.

2.3. Obtaining and treating mouse primary hepatocytes (MPHs)

MPHs were obtained as previously described [23]. Six-to-eight-week-old mice were anaesthetised and perfused through the inferior vena cava with 50 mL of Hank's buffer including 50 μM ethylene glycol tetraacetic acid and 50 mM HEPES (pH 7.4) for 10 min. Liver was separated from the mouse and digested for 2 min with type II collagenase (1 mg/mL) at 37 °C. The liver mixture was strained and washed for three times with plating medium. MPHs were placed in 12-well plates coated with collagen. After being cultured for 16 h, the MPHs were incubated with 0 or 5 mM APAP for 3, 12, and 24 h in Dulbecco's modified Eagle's medium (DMEM) (Hyclone, Hackensack, NJ, USA) without fetal bovine serum. APAP was dissolved in DMEM with 37 °C water bath and ultrasonic-assisted dissolution.

2.4. Serum alanine aminotransferase (ALT) and aspartate aminotransferase (AST) analysis

Blood was held at 4 °C for 2 h and then centrifuged to get serum. Serum ALT and AST were detected by appropriate enzymic kits (Zhongsheng Technologies, Beijing, China) as previous study described [22].

2.5. GSH measurement

The liver tissues were homogenized in 5% (*m*/*V*) trichloroacetic acid, then centrifuged at 2000 *g* for 10 min at 4 °C. The supernatant was used to measure the levels of reduced GSH in the liver using a total GSH/oxidized GSH assay kit from the Nanjing Jiancheng Bioengineering Institute (Nanjing, China), with the manufacturer's suggestions. Briefly, 10 μL of supernatant was mixed with 10 mM 5,5′-dithio-bis (2-nitrobenzoic acid) and the absorbance was detected at 405 nm after 30 s and 10.5 min to evaluate GSH content.

2.6. Malondialdehyde (MDA) measurement

The MDA can react with thibabituric acid (TBA) to form red product and can be detected at 532 nm. We evaluated MDA content by a kit from Nanjing Jiancheng Bioengineering Institute. Liver samples were ground with saline and centrifuged at 1600 *g* for 10 min at 4 °C. The supernatant was mixed with TBA reaction solution and water bathed at 95 °C for 40 min. After cooling, the supernatant absorbance was assessed at 532 nm.

2.7. Reactive oxygen species (ROS) measurement

We homogenized fresh liver tissues in homogenization buffer and centrifuged at 100 *g* for 5 min at 4 °C. 190 μL of supernatant was mixed with 10 μL of O08 probe and incubated at 37 °C in darkness for 30 min, then the fluorescence excitation/emission spectra were measured at 500/606 nm under a fluorescence microscope. A fluorescence intensity/protein concentration relationship was used to reflect liver ROS levels. The analysis kit was acquired from Bestbio Inc. (Shanghai, China).

2.8. Histological staining

After fixation in 10% (*V*/*V*) paraformaldehyde, the liver tissues were embedded in paraffin and sliced into sections that were 4-μm thick. The sections were stained via hematoxylin and eosin (H&E) according to the standard procedure to evaluate areas of necrosis.

2.9. Immunofluorescence

Fresh livers were used to make frozen sections with 8 μm. After fixing in 10% paraformaldehyde, livers were permeabilized in 0.2% (*V*/*V*) Triton X-100 for 30 min and blocked in phosphate-buffered saline (PBS) with 0.2% Triton X-100 and 5% (*V*/*V*) goat serum for 1 h. Sections were incubated with primary antibodies against Glrx1 (1:100 (*V*/*V*), 15804-1-AP; Proteintech) overnight at 4 °C. Then incubation of secondary antibodies (1:200 (*V*/*V*), 111-025-003; Jackson ImmunoResearch, West Grove, PA, USA) for 1 h at 37 °C followed three rounds of washing in PBS. After 4′,6-diamidino-2-phenylindole staining, sections were washed in PBS for three times and the images were captured using a fluorescence microscope (Nikon, Tokyo, Japan).

2.10. Extraction of RNA and quantitative real-time polymerase chain reaction (qPCR)

TRIzol reagent (Life Technologies, Carlsbad, CA, USA) was used to extract liver tissues and MPHs RNA, and PrimeScript™ RT reagent Kit (Takara, Otsu, Japan) was used to reverse-transcribe RNA into complementary DNA (cDNA). Finally, the cDNA was quantified by SYBR Green-based CFX96 reverse transcription-polymerase chain reaction (RT-PCR; Bio-Rad, Hercules, CA, USA). Table 1 shows the primer pairs used in the qPCR experiment.

Table 1
Primer sequences for quantitative real-time polymerase chain reaction (qPCR).

Genes	Forward (5′-3′)	Reverse (5′-3′)
Cyp1a2	ATCGGCAACCACGGCTTTCT	TGACCTGCCACT GGTTTATC
Cyp2e1	CCAACTCTGGACTCCCTTTTAT	ACGCCTTGAAATAGTCACTGTA
Cyp3a11	CTCAATGGTGTGTATATCCCC	CCGATGTTCTTAGACACTGCC
Gstp	GCGGCAAATATGTCACCCTC	GAAAGCTTTGCCTCCCTGG
Glrx1	AACAACACCAGTGCGATTCA	ATCTGCTTCAGCCGAGTCAT
Glrx2	GGCTCGGGAATGGGAAACAG	CGCATCTTGAA ACTGGTTGCC
Glrx3	CAGTGGTGGAAGTCGGCTC	GCCATGACATCGTTCATCTGT
Glrx5	TATGCGGCCTACAACGTGC	CCACTAGGTCCCCATTCTGAT
Il-6	CTGCAAGAGACTTCCATCCAG	AGTGGTATAGACAGGTCTGTTGG
Il-1β	GCAACTGTTCCTGAACTCAACT	ATCTTTTGGGGTCCGTCAACT
Mcp-1	GAGGACAGATGTGGTGGGTTT	AGGAGTCAACTCAGCTTTCTCTT
Tnfα	GGCGGTGC CTATGTCTCA	AGGGTCTGGGCCATAGAA
Trx1	TCCCTCCCCGCAACAGCCAA	ACCGGAGAACTCCCCCACCTTT
Trx2	TCGCCAAGCAGCACGGGAAG	CGGTAGGCACAGCTGACACCTCA
18s	TTGACTCAACACGGGAAACC	AGACAAATCGCTCCACCAAC

Cyp1a2: cytochrome p450 1a2; *Cyp2e1*: cytochrome p450 2e1; *Cyp3a11*: cytochrome p450 3a11; *Gstp*: glutathione *S*-transferase P; *Glrx1*: glutaredoxin-1; *Glrx2*: glutaredoxin-2; *Glrx3*: glutaredoxin-3; *Glrx5*: glutaredoxin-5; *Il-6*: interleukin-6; *Il-1β*: interleukin-1 beta; *Mcp-1*: monocyte chemoattractant protein-1; *Tnfα*: tumor necrosis factor alpha; *Trx1*: thioredoxin1; *Trx2*: thioredoxin2.

2.11. Western blotting

Liver tissues and MPHs were homogenized using radioimmune precipitation assay (RIPA) buffer (Beyotime Institute of Biotechnology, Nanjing, China). Protein concentration was assessed with bicinchoninic acid assay kit (Beyotime Institute of Biotechnology). A nitrocellulose membrane was used to transfer protein samples separated by 10% sodium dodecyl sulfate-polyacrylamide gel electrophoresis (SDS-PAGE) gels. 0.1% (*m*/*V*) casein is used to block membrane at room temperature for 1 h. We incubated the membranes overnight at 4 °C in the presence of antibodies, followed by 1 h at room temperature in the presence of a fluorescent secondary antibody. Finally, blots were detected using the LI-COR Odyssey System (LI-COR Biotechnology, Lincoln, NE, USA). The total liver PSSG analysis was performed as follows. The mice liver was homogenized using RIPA and added non-reducing protein sample loading buffer, and the samples were separated using 10% SDS-PAGE gel, and then incubated with anti-GSH overnight.

2.12. The enzyme-linked immunosorbent assay (ELISA)

The 50 mg of liver tissue sample was homogenized with 1 mL of PBS (containing 0.2% (*V*/*V*) Triton X-100), and the supernatant was obtained by centrifugation at 13,000 *g* for 20 min at 4 °C. Then, 100 μL of supernatant was assayed for mouse interleukin-1 beta (IL-1β) (88-7013-88), IL-6 (88-7064-88), and tumor necrosis factor alpha (TNFα) (88-7324-88) using the commercial ELISA kit (Invitrogen, Vienna, Austria) following the manufacturer's guidelines.

2.13. Immunoprecipitation

Liver tissues were homogenized in lysis buffer (20 mM Tris-hydrochloric acid, 150 mM NaCl, 10% (*V*/*V*) glycerol, and 1% (*V*/*V*) NP-40), and a protease inhibitor cocktail was added. In each case, 400 μg of protein was immunoprecipitated with anti-GSH overnight at 4 °C. Following this, the samples were incubated with 20 μL of Protein G Magnetic Beads (70024; Cell Signaling Technology) for 4 h at room temperature. After three washes with lysis buffer, the beads with the immune-precipitated complex were boiled at 100 °C for 10 min, and the eluted protein was separated via SDS-PAGE.

2.14. Measurements of APAP metabolites

The mice received APAP by intraperitoneal injection a dosage of 200 mg/kg after being fasted for 16 h. Blood was collected from each mouse's femoral vein at the following post-dose intervals: 0.25, 0.5, 1, and 3 h. After euthanizing the mice, blood and liver samples were obtained. The blood was stored in a tube with heparin sodium, and then separated to obtain plasma. The liver tissue was homogenized with saline. Until analysis, all samples were kept at a temperature of −80 °C.

The samples were prepared according to the following steps: 180 μL of cold methanol (Thermo Fisher Scientific Inc., Waltham, MA, USA) containing 50 ng/mL theophylline (inner stander, 1ST10355; Alta scientific co. Ltd., Tianjin, China) was added to 20 μL of plasma sample; each sample was then vortexed for 15 min and precipitated at −20 °C for half an hour. After centrifugation at 13,000 *g* twice for 20 min each time, 90 μL of supernatant was moved into the clean bottle; finally, 2 μL supernatant was injected into the analytical column for liquid chromatography tandem mass spectrometry (LC-MS/MS) analysis. For liver homogenates, 900 μL of cold methanol with theophylline (50 ng/mL) was added to 100 μL of liver homogenates. The subsequent process was the same as the plasma preparation mentioned above.

The AB Sciex Qtrap 6500+ ultra-high performance liquid chromatography-MS/MS (UPLC-MS/MS) system (AB Sciex, Redwood city, CA, USA) was used to analysis the concentrations of APAP and its metabolites. Chromatography was performed on an Acquity UPLC H-class system using an Acquity UPLC HSS T3 column (2.1 mm × 100 mm, 1.8 μm) (186003539; Waters, Milford, MA, USA). We used water with 0.1% (*V*/*V*) formic acid (Thermo Fisher Scientific Inc.) as the mobile phase A and pure acetonitrile (Thermo Fisher Scientific Inc.) as the mobile phase B. The optimized elution conditions were 10% (*V*/*V*) mobile phase B isocratic elution, with the flow rate of 0.3 mL/min for 7 min. Detection was conducted in positive electrospray ionization (ESI) mode. The target compounds were detected by measuring the *m*/*z* 152.1/110.3 for APAP, *m*/*z* 457.1/328.1 for APAP-GSH, *m*/*z* 232.3/152.1 for APAP-Sul, *m*/*z* 271.1/182.1 for APAP-CYS, and *m*/*z* 313.1/271.1 for APAP-NAC. The data analysis was done using the Analyst Software Version 1.6.3 (AB Sciex).

2.15. Liver microsome extraction and Cyp450 enzymes activity detection

Liver microsomes were separated by differential centrifugation. The sample was centrifuged at 10,000 *g* for 20 min at 4 °C, and then the supernatant was transferred to a clean tube and centrifuged again at 105,000 *g* for 1 h at 4 °C. Finally, the resulting precipitates were the liver microsomes.

The microsomes were quantified and incubated with a cocktail of substrate (phenacetin, midazolam, chlorzoxazone) and nicotinamide adenine dinucleotide phosphate regenerating reagent (PrimeTox Bio-pharma Technology Co., Ltd., Wuhan, China). The mixed reaction system was incubated at 37 °C for 1.5 min (midazolam) and 10 min (phenacetin and chlorzoxazone). The substrates and their specific products were assayed by UPLC-MS/MS. The detailed procedures were the same as previously described [24]. Finally, we analyzed the concentrations of the specific metabolites of substrates to evaluate Cyp450 enzymes activity.

2.16. Experimental design and statistical analysis

All animals were randomized for treatment. The operators of the examinations and data analyses were blinded. We presented the data as mean ± standard error of mean. Student's *t*-test (two experimental conditions) or the one-way analysis of variance multiple comparison test was used for statistical comparisons in GraphPad Prism 7 (GraphPad Software Inc., San Diego, CA, USA). Statistically significance was defined as $P < 0.05$.

3. Results

3.1. Hepatic expression of Glrx1 is decreased in mice with APAP-induced hepatotoxicity

To explore whether *S*-glutathionylation has impacts on APAP-caused hepatic injury, the content of total PSSG was investigated in an APAP-caused hepatic injury mice model. Our findings showed a substantial rise in hepatic PSSG levels in mice post-APAP injection (Fig. 1A). The main enzymes associated with PSSG are members of the *Glrx* and thioredoxin (*Trx*) families [14]. We thus examined the mRNA levels of these genes in the mouse liver and MPHs under APAP exposure. Our results indicated that only *Glrx1* expression was markedly decreased in mice after APAP injection for 12 h, whereas other genes, including *Glrx2*, *Glrx3*, *Glrx5*, *Trx1*, *Trx2* and glutathione *S*-transferase P (*Gstp*) were unchanged (Fig. 1B). The same results were presented in MPHs after APAP stimulation for 24 h (Fig. 1C). To further understand the changes of *Glrx1* in APAP caused liver damage, we examined the *Glrx1* mRNA expressions at different times following APAP administration. *Glrx1* mRNA expressions were significantly decreased at 3 h, and remained at low expression levels at 12 and 24 h in the liver (Fig. 1D) and MPHs (Fig. 1E) after APAP treatment. Western blotting and immunofluorescence also detected decreased expression of Glrx1 in the mouse hepatic following APAP administration (Figs. 1F and G). These data indicate that Glrx1 and PSSG may have an impact on APAP-caused hepatic injury.

3.2. Glrx1 deficiency aggravates APAP-caused hepatotoxicity

To directly examine the impact of Glrx1 on APAP-caused hepatic damage, we used CRISPR Cas9-mediated gene targeting to knockout the *Glrx1* gene and generate *Glrx1*$^{-/-}$ mice [17]. The expression of Glrx1 substantially decreased in the *Glrx1*$^{-/-}$ mice (Figs. S1B and C). After administering 200 mg/kg APAP to the mice, the Glrx1 deficiency enhanced APAP-triggered elevations of serum ALT and AST at 3, 6, and 12 h (Fig. 2A). H&E staining showed slight centrilobular necrosis in the liver of *WT* mice post-APAP administration for 3 h, and the necrosis area obviously expanded at 12 h post-APAP administration. *Glrx1*$^{-/-}$ mice displayed more extensive necrotic liver damage than *WT* mice after APAP injection for 3 and 12 h (Fig. 2B).

Oxidative stress is vital to the progress of APAP-caused hepatic damage, and APAP treatment can deplete GSH [7]. We evaluated the antioxidative capacity and found the level of reduced GSH in the *Glrx1*$^{-/-}$ mice were obviously lower in relation to the *WT* mice (Fig. 2C). The MDA, which is an indicator of oxidative stress, was higher in the *Glrx1*$^{-/-}$ mice after APAP treatment (Fig. 2D). Consistently, ROS was also significantly increased in the *Glrx1*$^{-/-}$ mice post-APAP administration (Fig. 2E). Studies have shown that exposure to APAP can activate the mitogen-activated protein kinase (MAPK) signaling pathway, especially activating JNK and promoting p-JNK translocation to mitochondria to aggravate its oxidative stress and damage [25]. To detect whether Glrx1 deficiency could affect MAPK pathways, we analyzed the phosphorylation levels of JNK and ERK. These data illustrate that the phosphor-ERK (p-ERK) and p-JNK were significantly elevated at 3 h in the *Glrx1*$^{-/-}$ mice after APAP treatment (Fig. 2F).

Prior research has shown that the severity of hepatic damage caused by APAP is associated with inflammatory infiltration [26]. To evaluate whether Glrx1 deficiency impacts

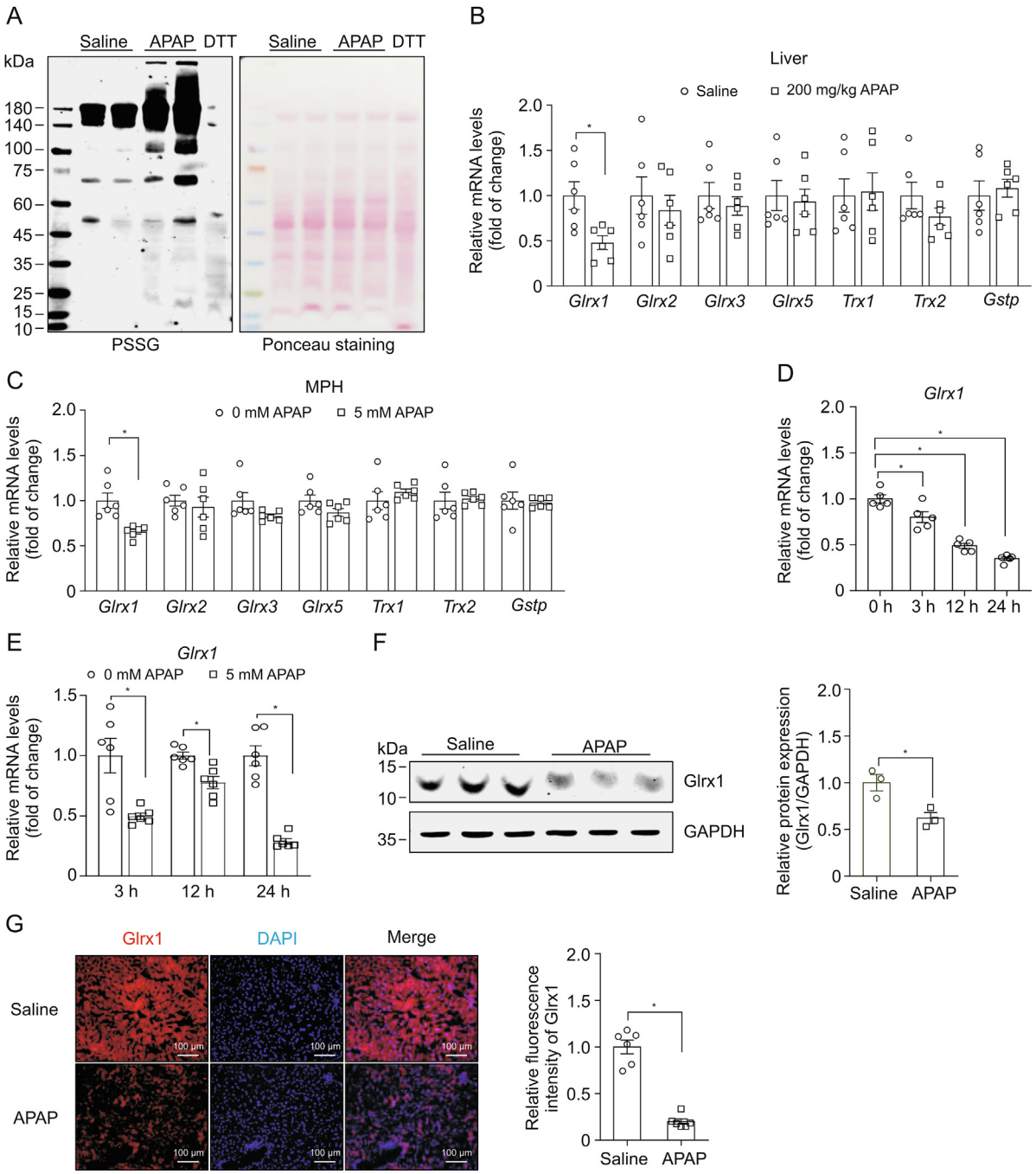

Fig. 1. Protein *S*-glutathionylation (PSSG) was involved in acetaminophen (APAP)-induced hepatotoxicity, and the expression of glutaredoxin-1 (Glrx1) was inhibited after APAP administration. (A) The total PSSG of the liver in wild type (*WT*) mice after APAP (200 mg/kg) treatment was detected under non-reducing conditions (left panel). Ponceau staining was used as a loading control (right panel). (B) Hepatic mRNA expression of genes related to PSSG in *WT* mice after APAP treatment for 12 h ($n = 6$). (C) mRNA expression of genes related to PSSG in mouse primary hepatocytes (MPHs). MPHs isolated from *WT* mice were cultured with 0 or 5 mM APAP for 24 h ($n = 6$). (D) Hepatic mRNA expression of *Glrx1* in mice after APAP treatment for 0, 3, 12, and 24 h ($n = 5$). (E) mRNA expression of *Glrx1* in MPHs treated with or without APAP for 3, 12, and 24 h ($n = 6$). (F) Hepatic protein expression of Glrx1 in mice after APAP treatment for 12 h (left panel) and quantifications of relative protein expression (right panel, $n = 3$). (G) Immunofluorescence staining of Glrx1 (red) and 4′,6-diamidino-2-phenylindole (DAPI) (blue) in the liver of *WT* mice after saline or 200 mg/kg APAP treatment for 24 h. Quantification are shown on the right ($n = 6$). Data are shown as mean ± standard error of mean. $^{*}P < 0.05$, two-tailed Student's *t*-test. DTT: dithiothreitol, *Gstp*: glutathione *S*-transferase P, *Trx*: thioredoxin.

inflammatory cytokines following APAP treatment, we examined inflammatory factors and found that the mRNA levels of *Il-1β*, *Il-6*, and *Tnfα* (Fig. 2G) and protein levels (Fig. 2H) of IL-1β, IL-6, and TNFα were markedly upregulated in the *Glrx1*$^{-/-}$ mice compared with *WT* mice post-APAP treatment. The levels of inflammatory factors showed no difference between the *WT* and *Glrx1*$^{-/-}$ mice with saline treatment (Figs. S1D and E). These results indicate that Glrx1 is fundamental to defend against APAP-caused liver damage by regulating oxidant stress and inflammatory response.

3.3. Glrx1 deficiency increases the production of toxic metabolites of APAP

To understand the mechanism about Glrx1 deficiency aggravated APAP-caused liver damage, we analyzed APAP metabolites in the

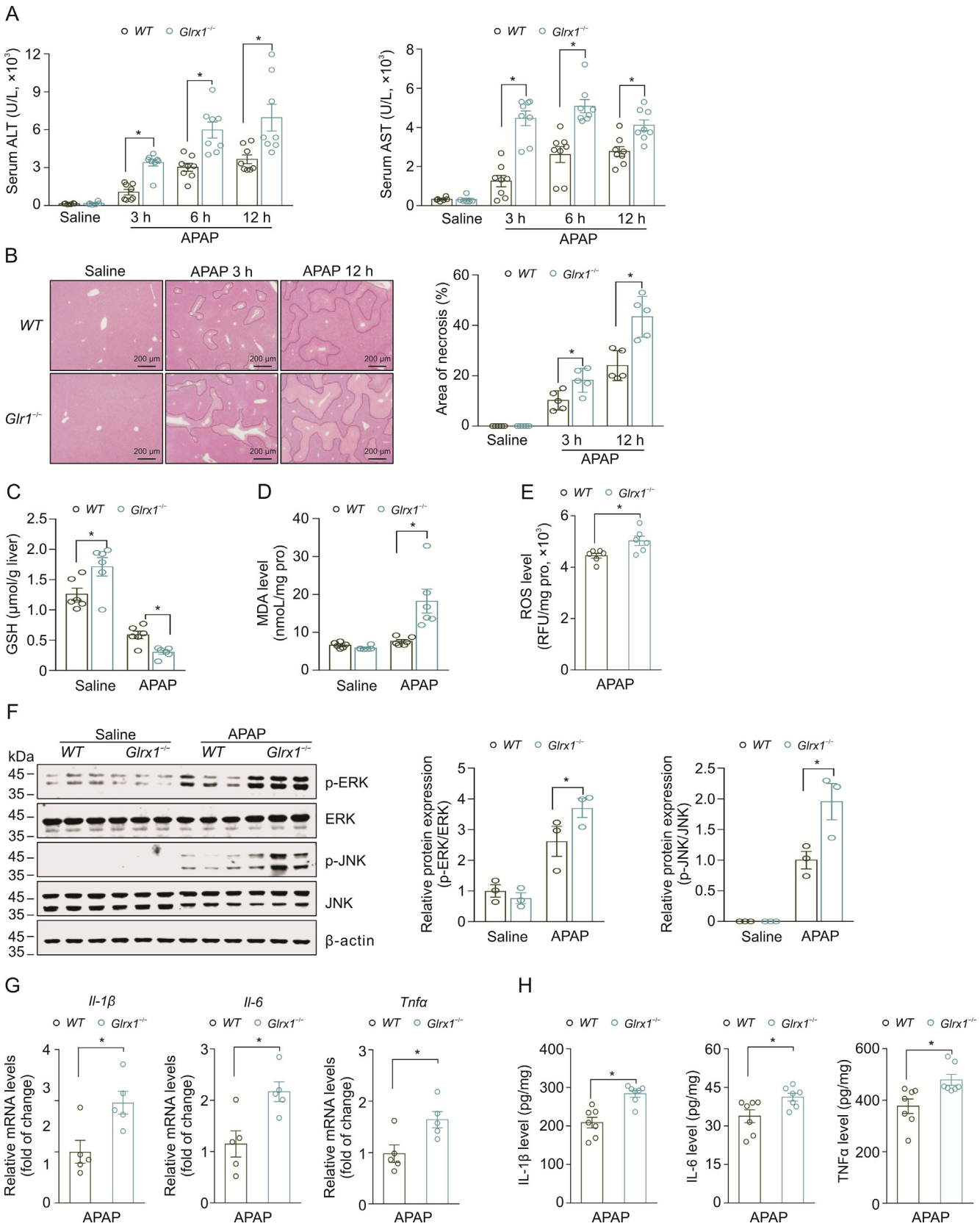

Fig. 2. Glutaredoxin-1 (Glrx1) ablation aggravated acetaminophen (APAP)-induced liver injury. Eight-to-ten-week-old male wild type (*WT*) and *Glrx1* knockout (*Glrx1*$^{-/-}$) mice were treated with saline or APAP (200 mg/kg) for 3, 6, and 12 h to induce hepatotoxicity. (A) Serum alanine aminotransferase (ALT) (left panel) and aspartate aminotransferase (AST) (right panel) levels at 3, 6, and 12 h (saline: $n = 6$, APAP: $n = 8$). (B) Representative hematoxylin and eosin staining of liver sections (3 and 12 h) and the quantifications of the necrosis areas ($n = 5$). (C) Hepatic reduced glutathione (GSH) content of mice after saline or APAP treatment for 3 h ($n = 6$). (D) Content of hepatic malondialdehyde (MDA) in mice after saline or APAP treatment ($n = 6$). (E) Relative hepatic content of reactive oxygen species (ROS) in mice after APAP treatment ($n = 6$). (F) Western blotting analysis of the protein

plasma and liver post-APAP administration. The primary metabolic routs of APAP and the metabolites are shown in Fig. 3A. *N*-acetyl-*p*-benzoquinone imine (NAPQI) is an active and unstable toxic metabolite not easily detected. The three metabolites APAP-GSH, APAP-CYS and APAP-NAC indicated the formation of the toxic metabolite NAPQI [27]. We analyzed the levels of APAP and its metabolites and found that there was no difference in APAP in the mouse plasma and liver between the *WT* and *Glrx1*$^{-/-}$ mice (Fig. 3B). The plasma concentration-time curve and area under the curve showed that the exposures of APAP-GSH, APAP-CYS and APAP-NAC in mouse plasma were significantly increased in the *Glrx1*$^{-/-}$ mice post-APAP administration for 3 h (left and middle panels, Figs. 3C–E). Consistently, the hepatic levels of these three metabolites were higher in the *Glrx1*$^{-/-}$ mice relative to the *WT* mice (right panel, Figs. 3C–E). Notably, the plasma and liver concentration of APAP-Sul was also significantly enhanced in *Glrx1*$^{-/-}$ mice (Fig. S1F). These results strongly indicate that absence of Glrx1 promotes the formation of toxic metabolites of APAP.

3.4. Glrx1 deficiency in mice increases the activity of Cyp3a11

It has been demonstrated that overdose APAP was metabolized to NAPQI via Cyp450 enzymes, including Cyp1a2, Cyp2e1, and Cyp3a11 [6]. Therefore, we detected the expression of Cyp450 enzymes and found that the mRNA and protein levels of Cyp1a2, Cyp2e1, and Cyp3a11 were comparable between the *WT* and *Glrx1*$^{-/-}$ mice after APAP and saline treatments S1G(Figs. 4A–C and S1G). Considering that enzyme activity is strongly associated with metabolic capacity, it is indispensable to assess Cyp450 enzymes activity. The data indicated that the relative activity of Cyp3a11 was obviously superior in the *Glrx1*$^{-/-}$ mice comparison with *WT* mice post-APAP injection, whereas the activities of Cyp1a2 and Cyp2e1 were consistent between the *WT* and *Glrx1*$^{-/-}$ mice (Fig. 4D). The protein expression of Cyp3a11 was unaltered, but its activity increased, which suggested other causes affected its activity, such as PTMs. It is well-known that PSSG is an important PTM and Glrx1 is an important enzyme of deglutathionylation [14,28]. We further detected the hepatic PSSG levels and found that the total hepatic PSSG of the *Glrx1*$^{-/-}$ mice was markedly elevated versus to the *WT* mice (Fig. 4E). Immunoprecipitation and subsequent western blotting demonstrated that the *S*-glutathionylation of Cyp3a11 was markedly elevated in the *Glrx1*$^{-/-}$ mice relative to *WT* mice (Fig. 4F). However, the *S*-glutathionylation of Cyp1a2 and Cyp2e1 was unchanged between the *WT* and *Glrx1*$^{-/-}$ mice (Figs. 4G and H). These data imply that the augmented *S*-glutathionylation of Cy3a11 in the *Glrx1*$^{-/-}$ mice may be responsible for the increased activity of Cyp3a11.

3.5. Liver-specific overexpression of Glrx1 alleviates APAP-caused hepatotoxicity by reducing the toxic metabolites of APAP

To further investigate the function of Glrx1 in APAP-caused liver damage, we constructed liver specific-overexpression *Glrx1* (*AAV8-Glrx1*) mice and control (*AAV8-GFP*) mice by injecting *AAV8*. We observed that Glrx1 expression was considerably enhanced after three weeks of virus injection (Fig. S2A). Mice with successful Glrx1 overexpression were starved for 16 h and received intraperitoneal injection of APAP (200 mg/kg). *AAV8-Glrx1* mice attenuated APAP-induced elevations of serum ALT and AST post-APAP administration for 3, 6, and 12 h (Fig. 5A). H&E staining indicated that *AAV8-Glrx1* mice exhibited less liver necrosis at 3 and 12 h post-APAP injection versus to *AAV8-GFP* mice (Fig. 5B). We evaluated the antioxidative capacity and found the level of reduced GSH in the *AAV8-Glrx1* mice was substantially enhanced than *AAV8-GFP* mice post-APAP administration for 3 h (Fig. 5C). Furthermore, the contents of hepatic MDA and ROS were significantly reduced in the *AAV8-Glrx1* mice (Figs. 5D and E). Western blotting results showed that APAP activated p-JNK and p-ERK were markedly inhibited in the *AAV8-Glrx1* mice (Fig. 5F). Following APAP treatment, the mRNA levels of inflammatory-response genes *Il-1β*, and *Tnfα* were markedly reduced in the *AAV8-Glrx1* mice (Fig. 5G), and the protein levels of IL-1β and IL-6 were reduced in the *AAV8-Glrx1* mice (Fig. 5H). Meanwhile, the mRNA and protein levels of inflammatory factors were consistent between the *AAV8-GFP* and *AAV8-Glrx1* mice with saline treatment (Figs. S2B and C).

To better understand the protective role of Glrx1-overexpression, we evaluated the levels of APAP and its primary metabolites. APAP levels showed no difference in the *AAV8-GFP* and *AAV8-Glrx1* mice post-APAP injection for 3 h (Fig. S2D). However, the plasma and liver contents of APAP-CYS and APAP-NAC significantly decreased in the *AAV8-Glrx1* mice at 3 h following APAP administration, despite no difference in the plasma and hepatic concentrations of APAP-GSH between the two groups (Figs. 6A and B), suggesting that the NAPQI formation was reduced in the *AAV8-Glrx1* mice. The plasma concentration of APAP-Sul was lower in *AAV8-Glrx1* group than *AAV8-GFP* group (Fig. S2E). The enzyme activity results showed that the hepatic Cyp3a11 activity of *AAV8-Glrx1* mice was lower than *AAV8-GFP* mice (Fig. 6C). Additionally, Glrx1 overexpression significantly decreased both the total PSSG of the liver (Fig. S2F) and the *S*-glutathionylation of Cyp3a11 (Fig. 6D). The mentioned results demonstrate that Glrx1-specific overexpression in the hepatic alleviates APAP-caused liver damage via inhabiting the Cyp3a11 activity and decreasing the toxic metabolites of APAP.

3.6. PFD pretreatment alleviates APAP-induced hepatotoxicity

Our earlier studies revealed that PFD significantly induced Glrx1 mRNA and protein expression in primary hepatic stellate cells. The anti-fibrosis effect of PFD was Glrx1 dependent, suggesting that Glrx1 is a therapeutic target of PFD [17]. Furthermore, our current studies indicated that PFD increased the mRNA and protein expression of Glrx1 in mice after APAP injection (Figs. 7A and B).

To evaluated the defensive effect of PFD on APAP-caused hepatic damage, we treated mice according to a schematic shown in Fig. S3A. The APAP-induced elevations of serum ALT and AST levels were considerably lower in the PFD treatment mice (Fig. 7C). The H&E staining results showed that liver necrosis areas were significantly reduced with PFD pretreatment at 3, 12, and 24 h following APAP injection (Fig. 7D). The antioxidative capacity results indicated that the content of reduced GSH was markedly higher in the PFD-treated mice in contrast to Veh group after APAP treatment (Fig. 7E). Western blotting results showed that PFD pretreatment obviously inhibited APAP-induced p-ERK and p-JNK activation (Figs. 7F and G). Following APAP treatment, the mRNA expressions of *Il-1β*, *Tnfα* and *Mcp-1* were significantly reduced in PFD-treated mice (Fig. 7H). Furthermore, after saline treatment, PFD was shown to decrease the mRNA expression of *Il-1β*, but did not change the expressions of *Tnfα* and *Mcp-1* (Fig. S3B). These results

expression of extracellular signal-regulated kinases (ERK), phosphor-ERK (p-ERK), c-Jun N-terminal kinase (JNK) and phosphor-JNK (p-JNK) (left panel) and the relative quantification of p-ERK ratio to ERK and p-JNK ratio to JNK (right panel, $n = 3$). (G) Relative mRNA expression ($n = 5$–6) and (H) protein levels ($n = 6$) of inflammatory factor interleukin-1 beta (IL-1β), IL-6, and tumor necrosis factor alpha (TNFα) in the liver after APAP treatment. Data are presented as mean ± standard error of mean. $^{*}P < 0.05$, two-tailed Student's *t*-test.

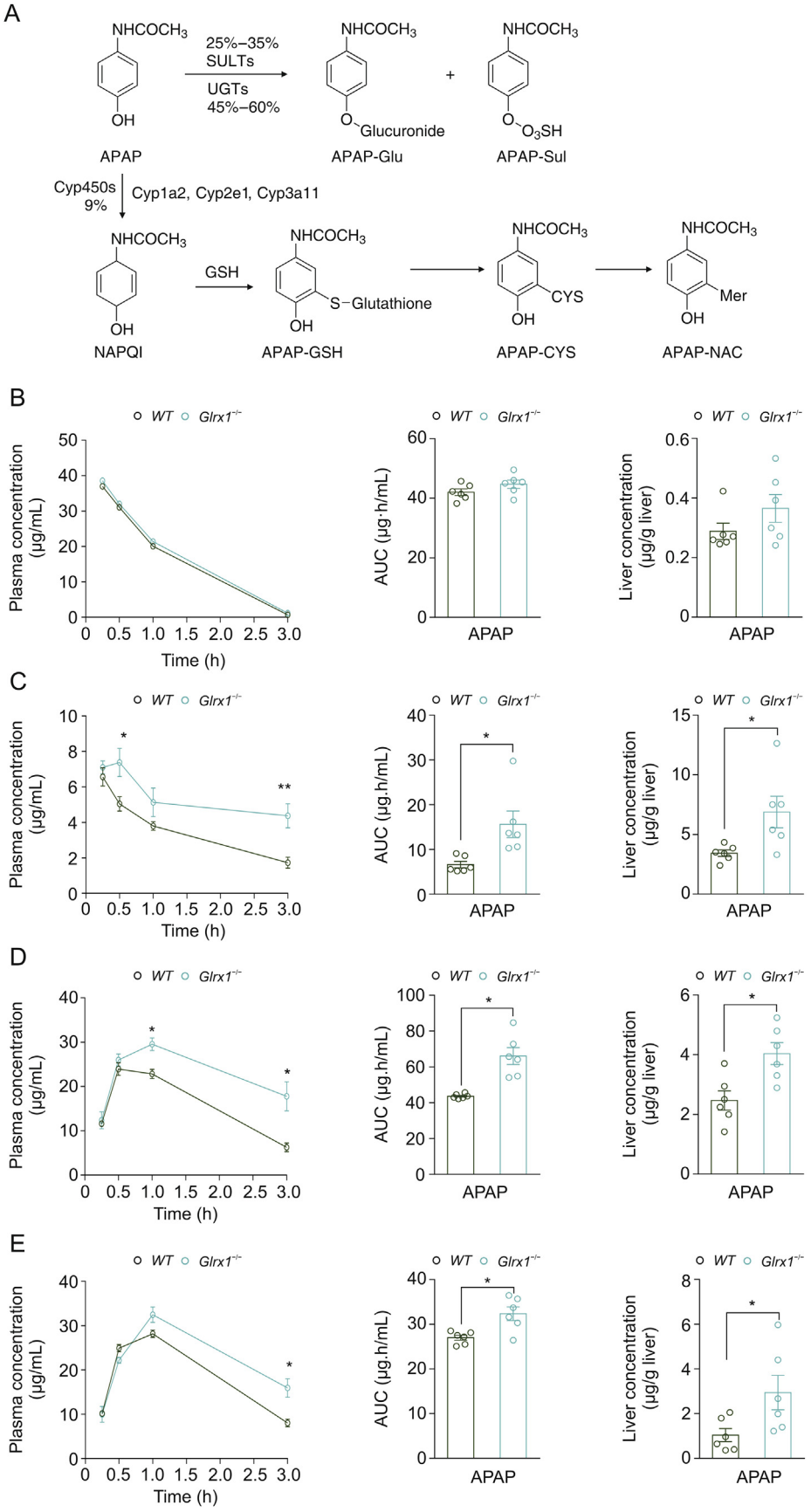

Fig. 3. Glutaredoxin-1 (Glrx1) ablation increased toxic metabolites of acetaminophen (APAP). (A) Schematic of APAP metabolism in the liver with three pathways. About 45%–60% of APAP are metabolized by phase II conjugating enzyme UDP-glucuronosyltransferases (UGTs) to form APAP-glucuronide (APAP-Glu); about 25%–35% are metabolized by phase II conjugating enzyme sulfotransferases (SULTs) to form APAP-sulfate (APAP-Sul); about 9% are metabolized by cytochrome P450 enzymes (Cyp450s), mainly cytochrome p450 1a2 (Cyp1a2), cytochrome p450 2e1 (Cyp2e1) and cytochrome p450 3a11 (Cyp3a11) to form *N*-acetyl-*p*-benzoquinone imine (NAPQI), and NAPQI is converted to APAP-glutathione (APAP-

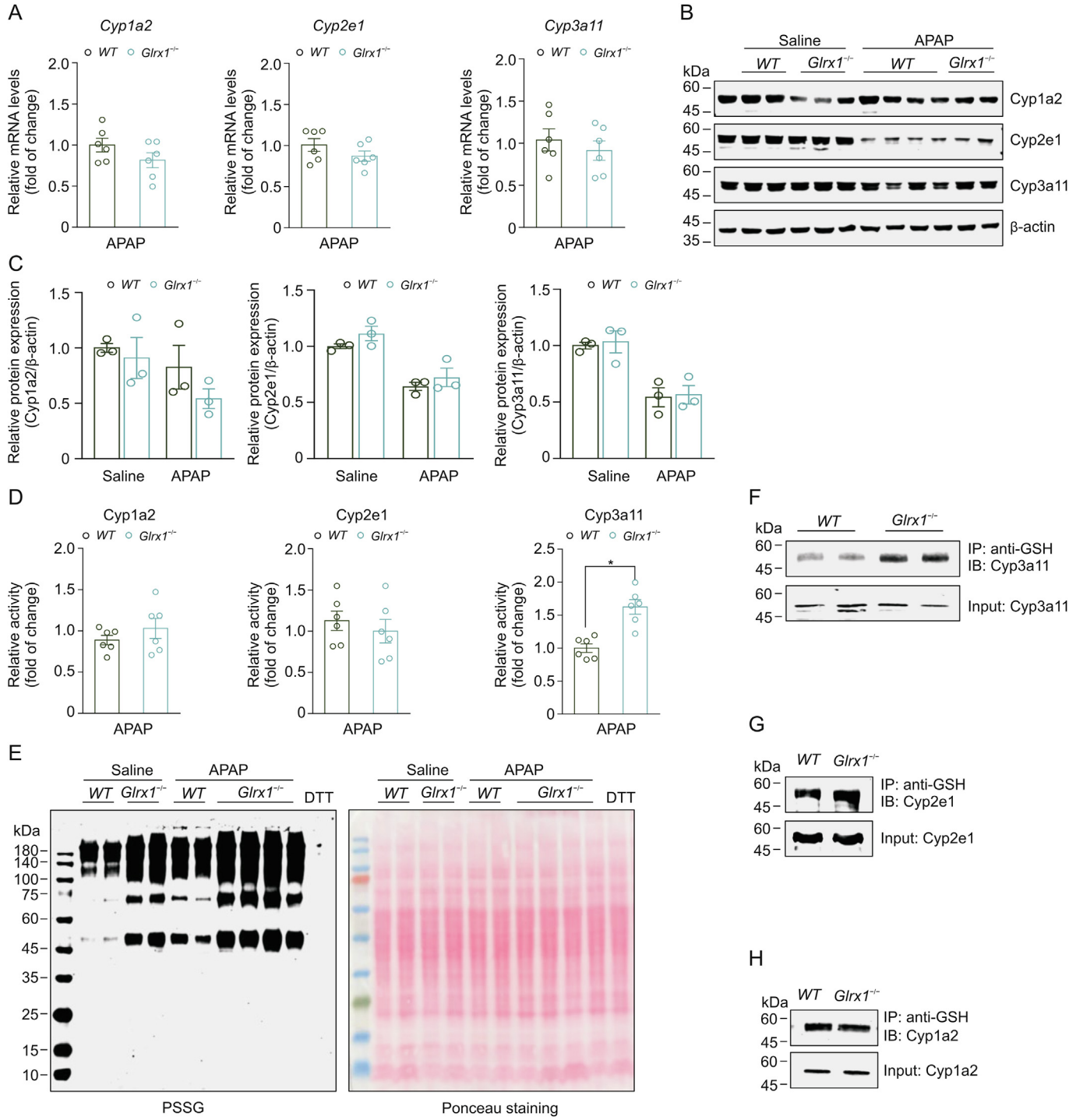

Fig. 4. The activity of cytochrome p450 3a11 (Cyp3a11) and its *S*-glutathionylation modification was increased in glutaredoxin-1 (Glrx1) deficiency mice. (A) mRNA expression of cytochrome p450 1a2 (*Cyp1a2*), cytochrome p450 2e1 (*Cyp2e1*) and *Cyp3a11* in the wild type (*WT*) and *Glrx1* knockout ($Glrx1^{-/-}$) mice after APAP treatment ($n = 6$). (B) Western blotting analysis of the hepatic protein expression of Cyp1a2, Cyp2e1 and Cyp3a11. (C) The relative quantification of Cyp1a2, Cyp2e1 and Cyp3a11 protein expression levels ($n = 3$). (D) Relative activity of Cyp1a2, Cyp2e1 and Cyp3a11 in liver microsomes ($n = 6$). (E) Hepatic protein *S*-glutathionylation (PSSG) in *WT* and $Glrx1^{-/-}$ mice under non-reducing conditions (left panel). Ponceau staining used as a loading control (right panel). (F–H) The *S*-glutathionylation of Cyp3a11, Cyp2e1 and Cyp1a2 in the *WT* and $Glrx1^{-/-}$ mouse liver samples were measured by immunoprecipitation with an anti-glutathione (anti-GSH) body, followed by the detection of anti-Cyp3a11 (F), anti-Cyp2e1 (G) and anti-Cyp1a2 (H) antibodies. Data are presented as mean ± standard error of mean. $^{*}P < 0.05$, two-tailed Student's *t*-test. DTT: dithiothreitol.

GSH), APAP-Cysteine (APAP-CYS) and 3-[*N*-acetyl-*L*-cystein-*S*-yl] acetaminophen (APAP-NAC). (B) Plasma concentration-time curves of APAP (left panel), plasma area under the curve (AUC) of APAP (middle panel), and liver concentration of APAP (right panel) in the wild type (*WT*) and *Glrx1* knockout ($Glrx1^{-/-}$) mice after APAP treated for 3 h ($n = 6$). (C) Concentration-time curves of APAP-GSH (left panel), plasma AUC of APAP-GSH (middle panel), and liver concentration of APAP-GSH (right panel) in the *WT* and $Glrx1^{-/-}$ mice after APAP treated for 3 h ($n = 6$). (D) Concentration-time curves of APAP-CYS (left panel), plasma AUC of APAP-CYS (middle panel), and liver concentration of APAP-CYS (right panel) in the *WT* and $Glrx1^{-/-}$ mice after APAP treated for 3 h ($n = 6$). (E) Concentration-time curves of APAP-NAC (left panel), plasma AUC of APAP-NAC (middle panel), and liver concentration of APAP-NAC (right panel) in the *WT* and $Glrx1^{-/-}$ mice after APAP treated for 3 h ($n = 6$). Data are presented as mean ± standard error of mean. $^{*}P < 0.05$, two-tailed Student's *t*-test.

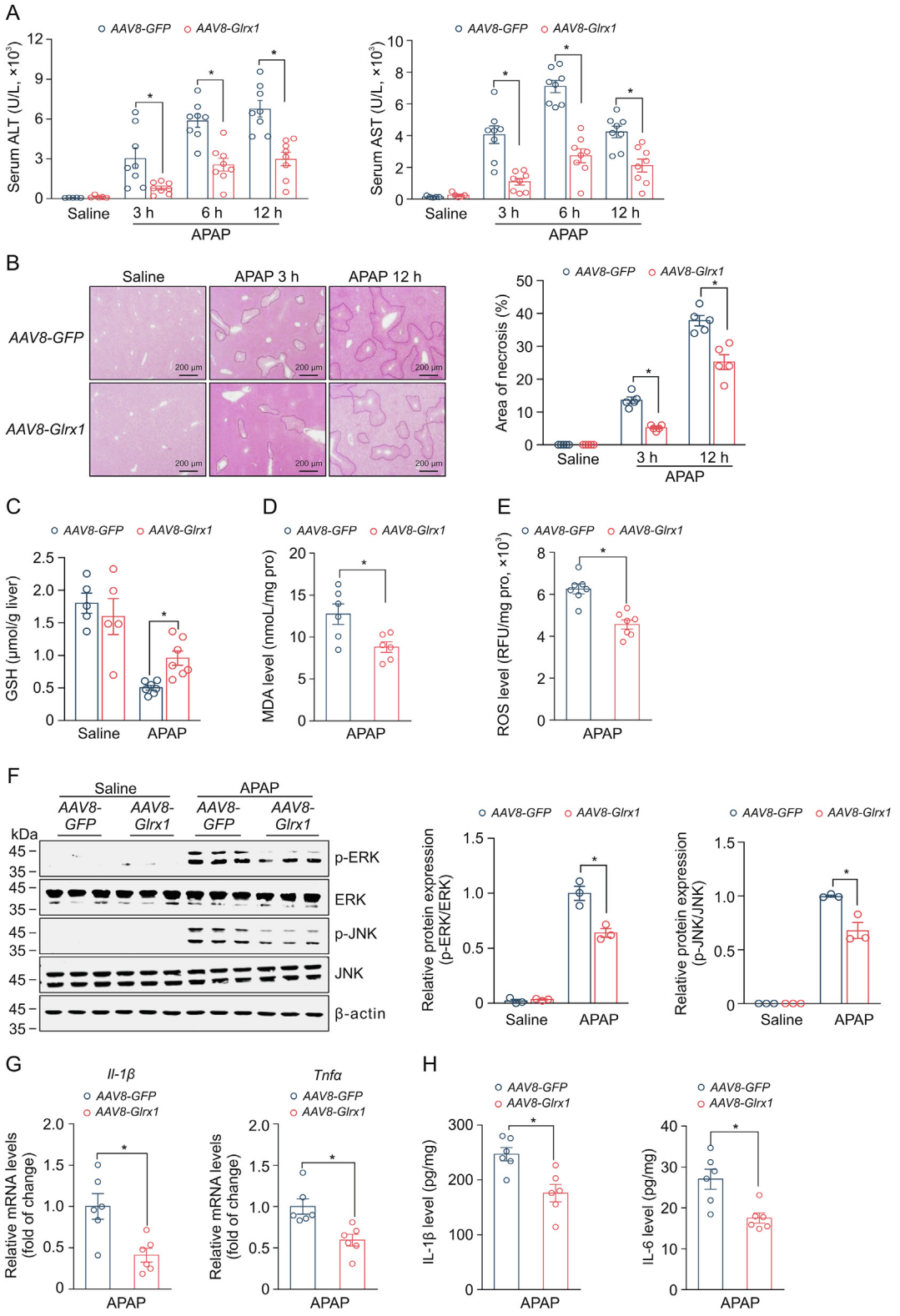

Fig. 5. Liver-specific overexpression of *Glrx1* (*AAV8-Glrx1*) alleviated acetaminophen (APAP)-induced hepatotoxicity. Eight-to-ten-week-old male control mice (*AAV8* vector containing only green fluorescent protein, *AAV8-GFP*) and *AAV8-Glrx1* mice were treated with saline or APAP (200 mg/kg) for 3, 6, and 12 h. (A) Serum levels of alanine aminotransferase (ALT) and aspartate aminotransferase (AST) (saline: $n = 5$, APAP: $n = 8$). (B) Representative hematoxylin and eosin staining and quantifications of necrosis areas of the liver sections at 3 and 12 h ($n = 5$). (C) Reduced glutathione (GSH) content of mice after saline or APAP treatment for 3 h (saline: $n = 5$, APAP: $n = 7$). (D) Hepatic content of malondialdehyde (MDA) in mice treated with APAP for 3 h ($n = 6$). (E) The relative hepatic level of reactive oxygen species (ROS) was measured by BBoxiProbe® O08 red probe after APAP challenge for 3 h ($n = 7$). (F) Western blotting analysis of the protein levels of extracellular signal-regulated kinases (ERK), phosphor-ERK (p-ERK), c-Jun N-terminal kinase (JNK) and phosphor-JNK (p-JNK) after APAP challenge for 3 h (left panel), and the quantification of p-ERK ratio to ERK and p-JNK ratio to JNK (right panel, $n = 3$). (G) Relative mRNA expression of interleukin-1 beta (*Il-1β*), tumor necrosis factor alpha (*Tnfα*) ($n = 6$). (H) Protein levels of IL-1β and interleukin-6 (IL-6) were measured by the enzyme-linked immunosorbent assay (ELISA) kits ($n = 6$). Data are presented as mean ± standard error of mean. $^{*}P < 0.05$, two-tailed Student's *t*-test.

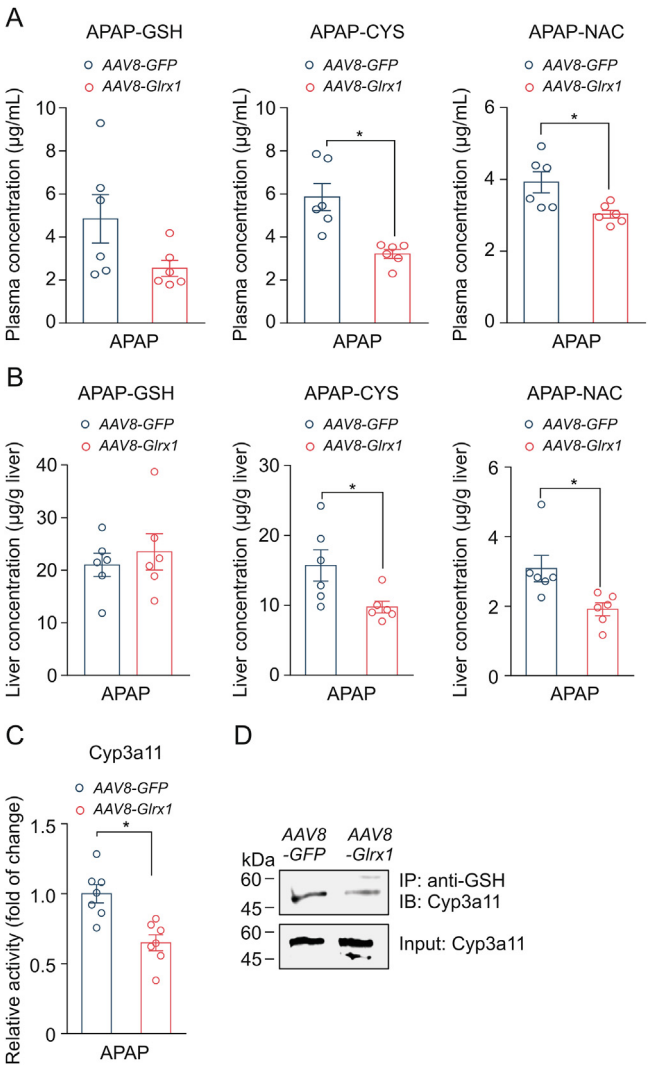

Fig. 6. Liver-specific overexpression of *Glrx1* (*AAV8-Glrx1*) reduced toxic metabolites of acetaminophen (APAP) and inhibited cytochrome p450 3a11 (Cyp3a11) activity. (A) Plasma concentration of APAP-glutathione (APAP-GSH) (left panel), APAP-Cysteine (APAP-CYS) (middle panel) and 3-[*N*-acetyl-*L*-cystein-*S*-yl] acetaminophen (APAP-NAC) in control (*AAV8* vector containing only green fluorescent protein, *AAV8-GFP*) mice and *AAV8-Glrx1* mice after APAP treatment for 3 h ($n = 6$). (B) Liver concentration of APAP-GSH (left panel), APAP-CYS (middle panel) and APAP-NAC (right panel) after APAP treatment for 3 h ($n = 6$). (C) Relative activity of cytochrome p450 3a11 (Cyp3a11) in liver microsomes ($n = 7$). (D) The *S*-glutathionylation of Cyp3a11 in *AAV8-GFP* and *AAV8-Glrx1* mouse liver samples. Data are presented as mean ± standard error of mean. $^{*}P < 0.05$, two-tailed Student's *t*-test.

demonstrate that the PFD pretreatment alleviates APAP-induced liver injury partly by increasing Glrx1 expression.

4. Discussion

At present, there is considerable research on APAP-caused hepatic damage, clarifying the mechanisms of APAP toxicity to a certain extent; however, a lack of effective therapeutic strategies remains. In this study, we characterized Glrx1 as an effective therapeutic target of APAP-caused hepatic damage. We found that Glrx1 deletion aggravated APAP-induced hepatotoxicity with higher levels of toxic metabolites of APAP, and that the increased activity of Cyp3a11 was accountable for the higher level of toxic metabolites. Glrx1 deletion increased the PSSG of the liver and increased the *S*-glutathionylation of Cyp3a11, which may be related to the increased activity of Cyp3a11. In contrast, the genetic and pharmacological induction of Glrx1 expression can attenuate the hepatotoxicity of APAP.

Glrx1 has been identified as an antioxidant protein, having a significant impact on oxidative stress [29,30]. Extensive oxidative stress is a character of APAP-caused liver damage. Furthermore, GSH is an antioxidant performing a vital effect on APAP stimulation, with a lack of GSH impairing the antioxidant defense of hepatocytes, thereby increasing the oxidative stress and cell damage [7,31]. In our study, after APAP treatment, the *Glrx1*$^{-/-}$ mice augmented the oxidative stress by depleting more reductive GSH than the *WT* mice and *AAV8-Glrx1* mice attenuated the oxidative stress by depleting less reductive GSH than the *AAV8-GFP* mice. Additionally, JNK phosphorylation can be triggered by oxidative stress and p-JNK translocate to mitochondria to trigger sustained ROS after APAP treatment [32,33]. ERK phosphorylation can also be induced by APAP treatment, and inhibiting its activation can alleviate APAP hepatotoxicity [13,34]. In our study, p-JNK and p-ERK were significantly induced by APAP treatment and Glrx1 deficiency enhanced the induction of p-JNK and p-ERK. Conversely, Glrx1 overexpression and PFD treatment inhibited the induction of p-JNK and p-ERK, suggesting that Glrx1 plays a vital role for oxidative states, p-JNK and p-ERK activation in APAP-caused hepatic damage.

It is common knowledge that excess NAPQI is the predominant reason for APAP-caused hepatotoxicity [35]. NAPQI is a highly reactive and unstable product that is difficult to be detected directly, and it can conjugate with GSH to product APAP-GSH. APAP-GSH is subsequently transformed to APAP-CYS and APAP-NAC, that are eventually eliminated through urination [36]. Prior studies have shown that NAPQI content can be indicated by concentrations of APAP-GSH, APAP-CYS and APAP-NAC [37–39]. Our results showed that NAPQI concentration was higher in the *Glrx1*$^{-/-}$ mice relative to the *WT* mice and lower in the *AAV8-Glrx1* mice than in the *AAV8-GFP* mice. This was associated with the levels of reductive GSH and states of p-JNK and p-ERK. It is revealed that Cyp1a2, Cyp2e1, and Cyp3a11 are mainly responsible for NAPQI formation [40]. Our results indicated that the increased activity of Cyp3a11 was responsible for NAPQI formation and protein PTMs affect Cyp3a11 activity.

S-glutathionylation is a ubiquitous redox modification and has a crucial function in oxidative stress conditions [41,42]. Previous studies have suggested that PSSG is a potential mechanism of APAP-caused hepatic damage [13]. Some investigations have demonstrated that the hepatic total PSSG is upregulated post-APAP administration [43], but the detailed functions of *S*-glutathionylation in APAP-caused hepatic damage are complicated. McGarry et al. [13] suggested that the *S*-glutathionylation of proteins mainly involving redox, metabolism and mitochondrial function can protect *Gstp1/2*$^{-/-}$ mice from APAP toxicity. Chan et al. [11] study found that *S*-glutathionylation resulted in the dysfunction of energy metabolism, increased oxidative stress and cytosolic calcium, and dysfunction of mitochondria to increase injury in HepaRG cells after APAP treatment. In present research, we observed that APAP induced hepatic PSSG and Glrx1 deficiency increased PSSG, by contrast, the overexpression of Glrx1 decreased PSSG. Glrx1 is a crucial glutathione-specific thioltransferase, being crucial to deglutathionylation [44]. Previous studies have revealed that Glrx1 regulates the *S*-glutathionylation of multiple proteins to inhibit or activate their functions [18,45,46]. In our study, Glrx1 deficiency significantly increased the *S*-glutathionylation of Cyp3a11, suggesting that the increased *S*-glutathionylation of Cyp3a11 might be responsible for its increased activity. Further experiments are required to understand the impact of *S*-glutathionylation modification on Cyp3a11 activity, including the identification and validation of the modification site.

PFD is an anti-fibrosis drug that is clinically used for idiopathic pulmonary fibrosis [47,48]. Our previous study demonstrated that

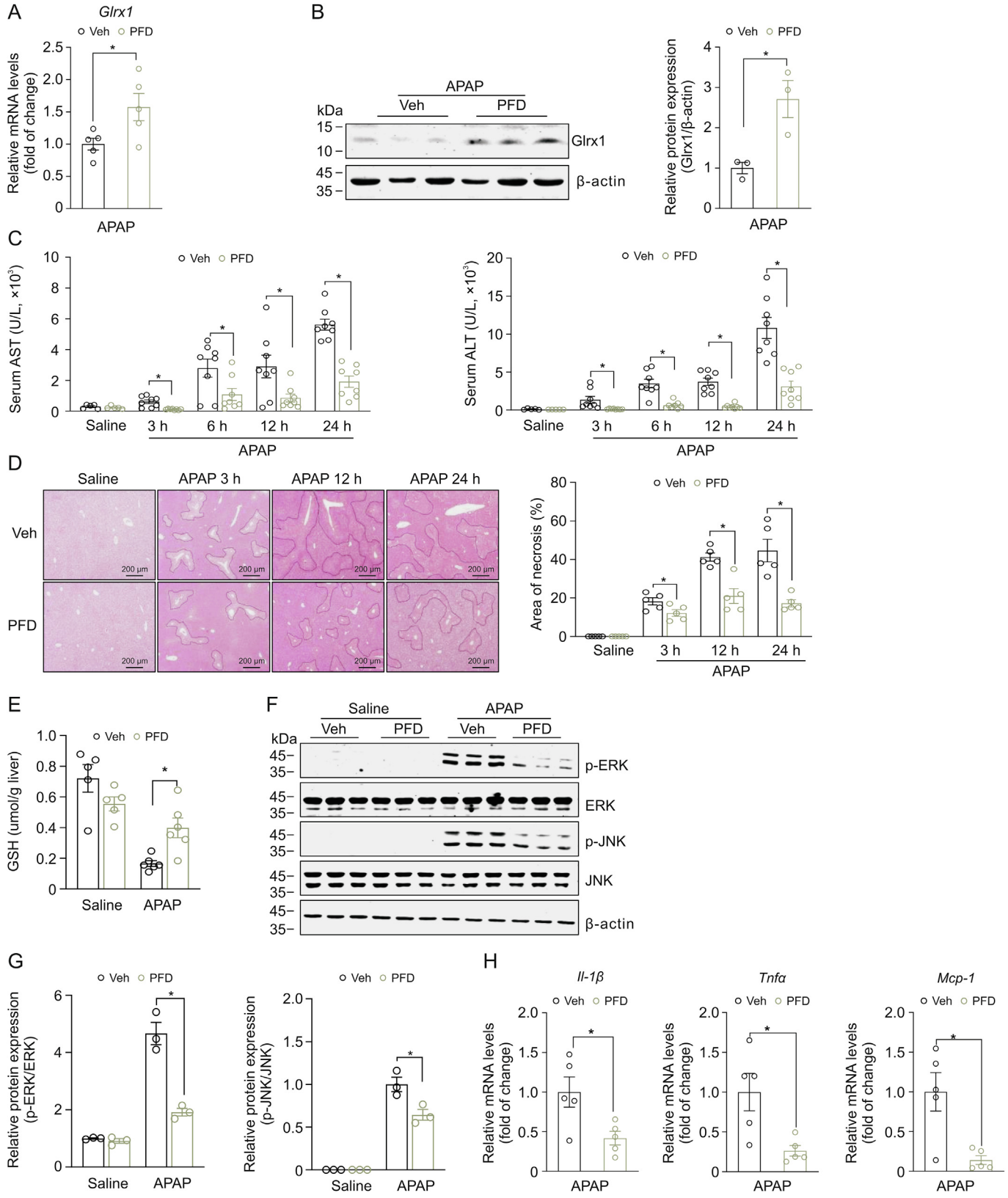

Fig. 7. Preceding treatment with pirfenidone (PFD) alleviated acetaminophen (APAP)-induced liver injury. (A) The mRNA expression of glutaredoxin-1 (*Glrx1*) in mice liver after PFD treatment ($n = 5$). (B) The protein expression of Glrx1 in mice liver, and the quantification of Glrx1 to β-actin after PFD treatment ($n = 3$). (C) Serum levels of alanine aminotransferase (ALT) and aspartate aminotransferase (AST) after APAP treatment (saline: $n = 5$, APAP: $n = 8$). (D) Representative hematoxylin and eosin staining of the liver sections at 3, 12, and 24 h (left panel) and quantifications of the necrosis areas (right panel, $n = 5$). (E) Relative hepatic content of reduced glutathione (GSH) of mice treated with saline or APAP for 3 h (saline: $n = 5$, APAP: $n = 6$). (F) Western blotting analysis of the protein levels of extracellular signal-regulated kinases (ERK), phosphor-ERK (p-ERK), c-Jun N-terminal kinase (JNK) and phosphor-JNK (p-JNK) after APAP challenge for 3 h. (G) The quantification of the expression ration of p-ERK to ERK and p-JNK to JNK ($n = 3$). (H) Relative mRNA expression of interleukin-1 beta (*Il-1β*), tumor necrosis factor alpha (*Tnfα*) and monocyte chemoattractant protein-1 (*Mcp-1*) after APAP treatment ($n = 5$). Data are presented as mean ± standard error of mean. $^{*}P < 0.05$, two-tailed Student's *t*-test.

PFD induced Glrx1 expression in hepatic stellate cells [17]. In our current study, PFD is shown to induce the expression of Glrx1 and decrease APAP-induced oxidative stress, p-JNK and p-ERK activation to alleviate APAP hepatotoxicity. These results demonstrate that PFD is a prospective therapeutic medicine for APAP hepatotoxicity. However, a limitation is that PFD was administered preceding APAP, which differs from the clinical scenarios. Future studies are required to explore the therapeutic benefits of PFD in the treating liver damage caused by APAP. In addition, the processes of APAP-caused liver damage are not exactly the same between mice and humans, and further studies related to humans are necessary to develop Glrx1 as a therapeutic target.

5. Conclusion

In summary, our study proves that Glrx1 is vital to APAP-induced hepatic damage. Glrx1 deficiency aggravates APAP-induced hepatotoxicity, which is associated with increased toxic metabolites of APAP. We find that Glrx1 deficiency increases the *S*-glutathionylation of Cyp3a11, likely increasing its activity. Additionally, the induction of Glrx1 by genetic technology and pharmaceutical preparation protect mice from APAP hepatotoxicity, suggesting a promising strategy to avoid and cure APAP hepatotoxicity.

CRediT author statement

Ying Xu: Conceptualization, Methodology, Investigation, Visualization, Writing - Original draft preparation, Reviewing and Editing; **Yan Xia:** Methodology, Validation, Investigation, Visualization, Writing - Reviewing and Editing; **Qinhui Liu:** Methodology, Resources, Investigation; **Xiandan Jing:** Methodology, Investigation; **Qin Tang:** Methodology, Funding acquisition; **Jinhang Zhang:** Methodology, Investigation; **Qingyi Jia:** Methodology, Investigation; **Zijing Zhang:** Methodology, Validation; **Jiahui Li:** Methodology, Validation; **Jiahao Chen:** Validation, Investigation; **Yimin Xiong:** Methodology, Validation; **Yanping Li:** Resources, Writing - Reviewing and Editing, Project administration, Funding acquisition; **Jinhan He:** Conceptualization, Resources, Supervision, Writing - Reviewing and Editing, Project administration, Funding acquisition.

Declaration of competing interest

The authors declare that there are no conflicts of interest.

Acknowledgments

This study was supported by the National Natural Science Foundation of China (Grant Nos.: 82025007, 81930020, and 82170874) and China Postdoctoral Science Foundation (Grant No.: 2022M710099). We appreciate professor Yao Chen and Jing Guo (Department of Clinical Pharmacology, Xiangya Hospital, Central South University) for their experimental supports, and Qianlun Pu (Advance Mass Spectrometry Center, West China hospital, Sichuan University) for the technical support.

Appendix A. Supplementary data

Supplementary data to this article can be found online at https://doi.org/10.1016/j.jpha.2023.08.004.

References

[1] W. Bernal, G. Auzinger, A. Dhawan, et al., Acute liver failure, Lancet 376 (2010) 190–201.
[2] A. Reuben, H. Tillman, R.J. Fontana, et al., Outcomes in adults with acute liver failure between 1998 and 2013: An observational cohort study, Ann. Intern. Med. 164 (2016) 724–732.
[3] A. Long, M. Magrath, M. Mihalopoulos, et al., Changes in epidemiology of acetaminophen overdoses in an urban county hospital after 20 years, Am. J. Gastroenterol. 117 (2022) 1324–1328.
[4] A. Bertolini, I.P. van de Peppel, F.A.J. A Bodewes, et al., Abnormal liver function tests in patients with COVID-19: Relevance and potential pathogenesis, Hepatology 72 (2020) 1864–1872.
[5] R.E. Moss, E.H. Hertzberg, H. Person, et al., Increase in rate of hospitalizations for pediatric intentional acetaminophen ingestion at a single center during the COVID-19 pandemic, Clin. Pediatr. 62 (2023) 295–300.
[6] M.R. McGill, H. Jaeschke, Metabolism and disposition of acetaminophen: Recent advances in relation to hepatotoxicity and diagnosis, Pharm. Res. 30 (2013) 2174–2187.
[7] K. Du, A. Ramachandran, H. Jaeschke, Oxidative stress during acetaminophen hepatotoxicity: Sources, pathophysiological role and therapeutic potential, Redox Biol. 10 (2016) 148–156.
[8] A. Ramachandran, H. Jaeschke, Acetaminophen hepatotoxicity, Semin. Liver Dis. 39 (2019) 221–234.
[9] B.H. Rumack, D.N. Bateman, Acetaminophen and acetylcysteine dose and duration: Past, present and future, Clin. Toxicol. 50 (2012) 91–98.
[10] A. Licata, M.G. Minissale, S. Stankevičiūtė, et al., N-acetylcysteine for preventing acetaminophen-induced liver injury: A comprehensive review, Front. Pharmacol. 13 (2022), 828565.
[11] J.C.Y. Chan, A.C.K. Soh, D.Y.Q. Kioh, et al., Reactive metabolite-induced protein glutathionylation: A potentially novel mechanism underlying acetaminophen hepatotoxicity, Mol. Cell. Proteom. 17 (2018) 2034–2050.
[12] X. Yang, J. Greenhaw, A. Ali, et al., Changes in mouse liver protein glutathionylation after acetaminophen exposure, J. Pharmacol. Exp. Ther. 340 (2012) 360–368.
[13] D.J. McGarry, P. Chakravarty, C.R. Wolf, et al., Altered protein *S-glutathionylation* identifies a potential mechanism of resistance to acetaminophen-induced hepatotoxicity, J. Pharmacol. Exp. Ther. 355 (2015) 137–144.
[14] A. Musaogullari, Y.C. Chai, Redox regulation by protein *S*-glutathionylation: From molecular mechanisms to implications in health and disease, Int. J. Mol. Sci. 21 (2020), 8113.
[15] R. Matsui, B. Ferran, A. Oh, et al., Redox regulation via glutaredoxin-1 and protein *S*-glutathionylation, Antioxid. Redox Signal. 32 (2020) 677–700.
[16] J.J. Mieyal, M.M. Gallogly, S. Qanungo, et al., Molecular mechanisms and clinical implications of reversible protein *S*-glutathionylation, Antioxid. Redox Signal. 10 (2008) 1941–1988.
[17] Y. Xi, Y. Li, P. Xu, et al., The anti-fibrotic drug pirfenidone inhibits liver fibrosis by targeting the small oxidoreductase glutaredoxin-1, Sci. Adv. 7 (2021), eabg9241.
[18] D. Shao, J. Han, X. Hou, et al., Glutaredoxin-1 deficiency causes fatty liver and dyslipidemia by inhibiting sirtuin-1, Antioxid. Redox Sign. 27 (2017) 313–327.
[19] M.I. Ahmad, M.U. Ijaz, M. Hussain, et al., High fat diet incorporated with meat proteins changes biomarkers of lipid metabolism, antioxidant activities, and the serum metabolomic profile in *Glrx1*$^{-/-}$ mice, Food Funct. 11 (2020) 236–252.
[20] X. Sun, C. Ye, Q. Deng, et al., Contribution of glutaredoxin-1 to Fas *S*-glutathionylation and inflammation in ethanol-induced liver injury, Life Sci. 264 (2021), 118678.
[21] K. Seidel, X. Wan, M. Zhang, et al., Alcohol binge drinking selectively stimulates protein *S*-glutathionylation in aorta and liver of ApoE$^{-/-}$ mice, Front. Cardiovasc. Med. 8 (2021), 649813.
[22] S. Pu, L. Ren, Q. Liu, et al., Loss of 5-lipoxygenase activity protects mice against paracetamol- induced liver toxicity, Br. J. Pharmacol. 173 (2016) 66–76.
[23] J. Yan, Q. Liu, Q. Tang, et al., Mesencephalic astrocyte-derived neurotrophic factor alleviates non-alcoholic steatohepatitis induced by Western diet in mice, FASEB J. 36 (2022), e22349.
[24] J. Guo, Y. Xu, L. Chen, et al., Gut microbiota and host Cyp450s co-contribute to pharmacokinetic variability in mice with non-alcoholic steatohepatitis: Effects vary from drug to drug, J. Adv. Res. 39 (2022) 319–332.
[25] E. Seki, D.A. Brenner, M. Karin, A liver full of JNK: Signaling in regulation of cell function and disease pathogenesis, and clinical approaches, Gastroenterology 143 (2012) 307–320.
[26] B.L. Woolbright, H. Jaeschke, Role of the inflammasome in acetaminophen-induced liver injury and acute liver failure, J. Hepatol. 66 (2017) 836–848.
[27] F.A. Schuran, C. Lommetz, A. Steudter, et al., Aryl hydrocarbon receptor activity in hepatocytes sensitizes to hyperacute acetaminophen-induced hepatotoxicity in mice, Cell. Mol. Gastroenterol. Hepatol. 11 (2021) 371–388.
[28] Y. Wang, P. Wang, Y. Zhang, et al., Decreased expression of the host long-noncoding RNA-GM facilitates viral escape by inhibiting the kinase activity TBK1 via *S*-glutathionylation, Immunity 53 (2020) 1168–1181.
[29] M. Okuda, N. Inoue, H. Azumi, et al., Expression of glutaredoxin in human coronary arteries, Arterioscler. Thromb. Vasc. Biol. 21 (2001) 1483–1487.
[30] N. Rouhier, J. Couturier, M.K. Johnson, et al., Glutaredoxins: Roles in iron homeostasis, Trends Biochem. Sci. 35 (2010) 43–52.
[31] C. Saito, C. Zwingmann, H. Jaeschke, Novel mechanisms of protection against acetaminophen hepatotoxicity in mice by glutathione and N-acetylcysteine, Hepatology 51 (2010) 246–254.

[32] S. Win, T.A. Than, R.W. M Min, et al., C-Jun N-terminal kinase mediates mouse liver injury through a novel Sab (SH_3BP_5)-dependent pathway leading to inactivation of intramitochondrial Src, Hepatology 63 (2016) 1987–2003.
[33] A. Ramachandran, H. Jaeschke, A mitochondrial journey through acetaminophen hepatotoxicity, Food Chem. Toxicol. 140 (2020), 111282.
[34] A.A. Widjaja, J. Dong, E. Adami, et al., Redefining IL11 as a regeneration-limiting hepatotoxin and therapeutic target in acetaminophen-induced liver injury, Sci. Transl. Med. 13 (2021), eaba8146.
[35] L.P. James, P.R. Mayeux, J.A. Hinson, Acetaminophen-induced hepatotoxicity, Drug Metab. Dispos. 31 (2003) 1499–1506.
[36] E. Yoon, A. Babar, M. Choudhary, et al., Acetaminophen-induced hepatotoxicity: A comprehensive update, J. Clin. Transl. Hepatol. 4 (2016) 131–142.
[37] P. Xu, Y. Xi, P. Wang, et al., Inhibition of p53 sulfoconjugation prevents oxidative hepatotoxicity and acute liver failure, Gastroenterology 162 (2022) 1226–1241.
[38] Y. An, P. Wang, P. Xu, et al., An unexpected role of cholesterol sulfotransferase and its regulation in sensitizing mice to acetaminophen-induced liver injury, Mol. Pharmacol. 95 (2019) 597–605.
[39] T. Zhang, F. Yu, L. Guo, et al., Small heterodimer partner regulates circadian cytochromes p450 and drug-induced hepatotoxicity, Theranostics 8 (2018) 5246–5258.
[40] A. Vonada, A. Tiyaboonchai, S. Nygaard, et al., Therapeutic liver repopulation by transient acetaminophen selection of gene-modified hepatocytes, Sci. Transl. Med. 13 (2021), eabg3047.
[41] S. Vrettou, B. Wirth, *S*-glutathionylation and *S*-nitrosylation in mitochondria: Focus on homeostasis and neurodegenerative diseases, Int. J. Mol. Sci. 23 (2022), 15849.
[42] R.J. Mailloux, J.R. Treberg, Protein *S*-glutathionlyation links energy metabolism to redox signaling in mitochondria, Redox Biol. 8 (2016) 110–118.
[43] J. Li, P. Cheng, S. Li, et al., Selenium status in diet affects acetaminophen-induced hepatotoxicity via interruption of redox environment, Antioxid. Redox Signal. 34 (2021) 1355–1367.
[44] F.T. Ogata, V. Branco, F.F. Vale, et al., Glutaredoxin: Discovery, redox defense and much more, Redox Biol. 43 (2021), 101975.
[45] V. Anathy, S.W. Aesif, A.S. Guala, et al., Redox amplification of apoptosis by caspase-dependent cleavage of glutaredoxin 1 and *S*-glutathionylation of Fas, J. Cell Biol. 184 (2009) 241–252.
[46] K. Dong, M. Wu, X. Liu, et al., Glutaredoxins concomitant with optimal ROS activate AMPK through *S*-glutathionylation to improve glucose metabolism in type 2 diabetes, Free Radic. Biol. Med. 101 (2016) 334–347.
[47] G. Sgalla, E. Cocconcelli, R. Tonelli, et al., Novel drug targets for idiopathic pulmonary fibrosis, Expert Rev. Respir. Med. 10 (2016) 393–405.
[48] L.H. Lancaster, J.A. de Andrade, J.D. Zibrak, et al., Pirfenidone safety and adverse event management in idiopathic pulmonary fibrosis, Eur. Respir. Rev. 26 (2017), 170057.